ELSEVIER

International Journal of Mass Spectrometry and Ion Processes 159 (1996) 125–136

International Journal of Mass Spectrometry and Ion Processes

Spectroscopy and photodissociation of size-selected $(CH_3I)_n^+$ cluster ions

Jack A. Syage*, Jhobe Steadman[1]

The Aerospace Corporation, P.O. Box 92957, Mail Stop M5-754, Los Angeles, CA 90009, USA

Received 12 March 1996; accepted 25 April 1996

Abstract

The resonant photodissociation of $(CH_3I)_n^+$ cluster ions (n = 1–5) was studied in a crossed molecular–electron–laser beam apparatus. These results were complemented by a study of the ionization/dissociation as a function of variable energy electron ionization (EI). The fragmentation that first appears as the EI energy is raised is loss of CH_3. This channel is particularly strong for n = 3. The lower energy dissociation of neutral I, on the other hand, is essentially quenched for cluster sizes of $n > 2$. Intermolecular dissociation (evaporation) of CH_3I was evident, but was not extensive, based on a minor sensitivity of the cluster ion distribution to EI energy. The photodissociation of $(CH_3I)_n^+$ resulted in different dissociation behavior than for EI. Resonant excitation of monomer CH_3I^+ to the predissociative A electronic state gave only $I + CH_3^+$. A state excitation of the cluster ions, on the other hand, resulted only in intermolecular dissociation. The photoexcitation cross-sections for the $A\ ^2E_{1/2} \leftarrow X\ ^2E_{1/2}$ transition are presented as a function of cluster size n. A two-photon dissociation channel is also identified and the cross-sections and dissociation products are reported. Finally, the frequency resolved photofragment excitation spectra of CH_3I^+ and $(CH_3I)_2^+$ are compared.

Keywords: Mass-specific cluster ion photodissociation; Photodissociation cross-sections; Electron ionization/dissociation; Low-mass rejection filter

1. Introduction

The study of atomic and molecular cluster properties is motivated to a large extent by the opportunities to investigate the transition from gas phase to bulk phase behavior [1]. This burgeoning field of study can be viewed as proceeding along two major branches. One direction is driven, for the most part, by the desire to better understand the structure and bonding that occurs as the clusters grow in size. A second major direction involves the chemical properties of clusters. We shall restrict our attention here to molecular cluster chemistry. An emerging field of molecular cluster work seeks to address how the addition of solvent molecules, one at a time, modifies the behavior of chemical reactions [2–4]. Important topics include understanding how unimolecular and bimolecular gas phase reactions are modified by stepwise solvation or how large must a solvent shell be to make a solution phase reaction energetically favorable. Seeded clusters have great appeal because they represent an environment that is intermediate between the gas phase and the condensed phase.

* Corresponding author.
[1] Present address: GeoCenters, Inc., Gun Powder Branch, P.O. Box 68, Aberdeen Proving Grounds, Maryland 21010, USA.

PII S0168-1176(96)04446-1

In this special issue on "Ion Spectroscopy", we are interested in the photochemistry that occurs in cluster ions as a function of cluster size. The study of size-specific photodissociation of clusters has progressed considerably in recent years as a result of new tandem time-of-flight (TOF) arrangements that isolate specific cluster ion sizes for photodissociation, and mass-resolve the resultant photofragments. The photodissociation of specific cluster sizes leads to fragmentation patterns that can be interpreted to reveal information about structure and bonding. The first studies of this kind involved metastable decay of neat cluster ions formed by nonresonant multiphoton ionization/dissociation and monitored by reflectron TOF devices. Castleman and coworkers, for example, unraveled many details concerning $(NH_3)_n^+$ and $(CH_3OH)_n^+$ metastable dissociation [5]. The reflectron studies are sensitive to metastable dissociations that occur on the timescale of the ion drift times (1–100 μs). For identifying products resulting from fast kinetics other techniques are needed.

We present our work on the size-specific photodissociation and fragmentation of $(CH_3I)_n^+$ cluster ions. The principal results made use of a technique in which a standard three-grid TOF mass spectrometer is operated as a tunable low mass rejection (LMF) filter. This adaptation has the capability of eliminating successively larger cluster sizes from the photodissociation region, thus making possible the sensitive detection of size-specific cluster ion photodissociation against a zero background. The LMF technique has been described before [6–8] and preliminary results on $(CH_3I)_n^+$ photodissociation were also reported [8]. Here, we present a more detailed study of size-specific $(CH_3I)_n^+$ photodissociation. This work is augmented by measurements of the cluster size dependent relative cross-sections for ion dissociation following variable energy electron ionization.

The molecule CH_3I was chosen for these studies because of its rich variety of dissociation mechanisms. It has also proved to be a popular subject of polyatomic ion studies, hence, a considerable amount of information is known about the monomer ion dissociation pathways [9–13]. Finally, unusually high resolution electronic state spectroscopy exists for CH_3I^+ [14,15], and the higher electronic energy states are reasonably well known [9]. These studies form a valuable body of information for interpreting the cluster ion properties. Although the monomer and cluster ions exhibit certain similarities, we were most intrigued by the differences observed in the reactivity between monomer and cluster ions as well as the pronounced dependence of many properties on cluster size. Results are also presented on the frequency-resolved photofragment excitation spectra of CH_3I^+ and $(CH_3I)_2^+$ as well as evidence for double excitation in the cluster species that precedes photodissociation.

2. Experimental

The apparatus used in the present experiments, shown in Fig. 1, is designed for the crossing of a molecular and electron beam pulse, and the subsequent crossing of the laser photodissociation pulse with the mass-filtered ionization volume. We have described many of the experimental details in previous work [6–8,16]. The molecular beam time-of-flight (TOF) mass spectrometer is a conventional design consisting of differentially pumped source and ionization chambers. In this work, we employed the following expansion conditions: Approximately 4% CH_3I in 25 psi Ar, 500 μm nozzle diam., 2 cm nozzle–skimmer distance, and 400 μs pulse width. At 10 Hz operation, the ionization chamber pressure increased to about 2×10^{-7}. The TOF mass spectrometer in Fig. 1 consists of the Wiley and McLaren three-grid ion optics configuration [17] (with 1 cm spacing) and a 1 m field-free drift tube. We use the symbols V0–V4 as a label for each grid in Fig. 1 and to represent the value of the DC voltage applied to each grid. Typical values are 0, 1500, 1500, 1400, and 1430 V, respectively.

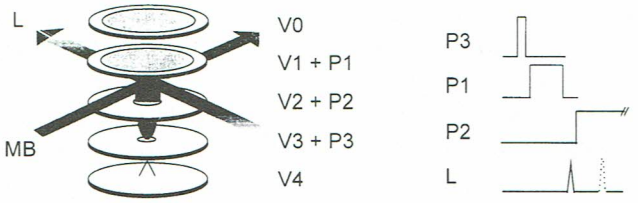

Fig. 1. Schematic of the crossed molecular–electron–laser beam ion optics assembly. Thermionic emission from a hairpin filament on grid V4 is the source of the electron beam. An electron pulse is gated on by P3. After ionization, the low mass filter (LMF) is activated by P1. The final pulse P2 reverses the direction of the remaining ions. Laser excitation L follows, and the parent and fragment ions are sampled in the time-of-flight mass spectrometer (TOFMS). The laser pulse L is shown for two different relative delays.

We note that the ionization region between V1 and V2 is nominally field-free and that the negative field across V3–V4 prevents electrons from exiting the filament region.

The basic principle for operating a three-grid ion optics assembly as a tunable low mass filter (LMF) is shown in Fig. 1 [7,8]. An electron pulse is admitted to the ionization region by applying the P3 pulse (typically 40 V, 0.4 μs) to grid V3. Following ionization, the P1 pulse (typically 20–80 V, 1–4 μs) is activated creating a negative field across V2–V3 that accelerates ions in a direction away from the detector. The lighter masses, which travel at higher velocities, are the first to exit the extraction region through the lower grid. After an appropriate time, the negative field gradient is reversed as P1 turns off and the P2 pulse is turned on. Ions above a threshold mass value are turned around and accelerated toward the detector in the usual manner.

A series of mass spectra, illustrating the operation of the LMF, is presented in Fig. 2. A normal mass spectrum of $(CH_3I)_n$ is plotted in Fig. 2(a). Operation of the LMF results in a TOF mass spectrum that is free of signal from ions below an adjustable threshold mass value m_0 (Fig. 2(b)). The cutoff mass is adjusted by varying the P1 voltage and when necessary the duration. A mass spectrum for a specific mass can be obtained by taking the difference spectrum for different settings of the threshold mass value. An example is given in Fig. 2(c) showing only dimer signal. The photodissociation of the selected higher ion masses produces lighter fragment masses that are detected against a zero background. The difference signal for $(CH_3I)_2^+$ with photolysis laser on gives a cluster size specific photofragment mass spectrum (Fig. 2(d)).

The electron ionization (EI) energies were calibrated against the known EI thresholds of He to He^+ and Ar to Ar^+ and Ar^{+2}. The electron

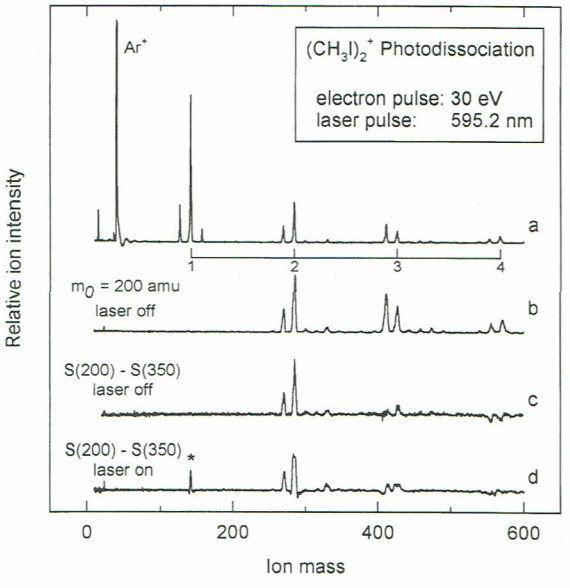

Fig. 2. Photodissociation of mass-selected $(CH_3I)_2^+$ at 595 nm. (a) 30 eV electron ionization mass spectrum of $(CH_3I)_n$ clusters. (b) The LMF rejects ions below mass 200 amu to give spectrum S(200). (c) The difference spectrum for LMF thresholds of 350 and 200 amu shows the presence of dimer cation peaks only. (d) The corresponding difference spectrum in the presence of laser photolysis (595.2 nm, 35 mJ per pulse, unfocused). The deflector voltages were adjusted to enhance the detection of larger clusters in these spectra and in Figs. 3 and 6.

energy resolution depends on maintaining field-free condition throughout the ionization region. The V2 potential was trimmed to compensate for the V0 ground grid penetrating V1. This was achieved by setting a 4 μs delay between ionization and ion extraction and measuring the drift of He^+ out of the extraction region due to residual fields. The V2 potential was adjusted with about 100 mV accuracy to minimize the He^+ drift and thereby maximize the detected ion signal. This procedure ensures a field gradient across the molecular beam of less than 50 mV.

The photodissociation pulses enter the chamber either unfocused or defocused so that the beam diameter at the excitation region (3–5 mm) can be closely matched to the overlap of the molecular beam and the electron beam. Pulse energies were varied from 1 to 40 mJ per pulse. The range of excitation was 532–610 nm. Cation excitation spectra are normalized to laser intensity (unless otherwise indicated) and represent single traces at a scan rate of about 0.24 nm min^{-1}, a pulse repetition rate of 10 Hz, and an effective integrating constant of about 0.05 nm. The pulse sequence diagrammed in Fig. 1 required external triggering of the laser Q-switch in order to synchronize the laser pulse to the EI ionization pulse, the LMF rejection pulse, and the subsequent ion extraction pulse.

3. Results

The major dissociation channels for $(CH_3I)_n^+$ cluster ions are summarized as follows:

$$(CH_3I)_n^+ \rightarrow (CH_3I)_{n-m}^+ + m(CH_3I) \quad (1)$$

$$(CH_3I)_n^+ \rightarrow I(CH_3I)_{n-1}^+ + CH_3 \quad (2)$$

$$(CH_3I)_n^+ \rightarrow I(CH_3I)_n + CH_3^+ \quad (3)$$

$$(CH_3I)_n^+ \rightarrow CH_3(CH_3I)_{n-1}^+ + I \quad (4)$$

$$(CH_3I)_n^+ \rightarrow CH_3(CH_3I)_n + I^+ \quad (5)$$

The designation m in reaction (1) does not necessarily imply fully dissociated neutral monomer fragments; some smaller neutral clusters could occur. A less prominent pathway due to neutral H atom dissociation is not treated here because unit mass resolution was not achievable for the cluster species using EI ionization. We also do not distinguish whether the neutral fragments shown above dissociate further, such as $I(CH_3I)_n$ to $I + (CH_3I)_n$ or $CH_3(CH_3I)_n$ to $CH_3 + (CH_3I)_n$. Only ions are monitored in this work.

In the following subsections we provide experimental evidence for the following conclusions: For EI/dissociation, reaction (2) is significant for all n studied, reaction (4) is significant only for $n \leq 2$. Reaction (1) occurs for all n, however, the extent of reaction is difficult to measure. For $A \leftarrow X$ photoexcitation of $(CH_3I)_n^+$, reaction (4) dominates for $n = 1$ and is absent for $n > 1$, being replaced exclusively by the intermolecular dissociation reactions (1).

3.1. Electron ionization/dissociation

Measurements of size-specific photodissociation of $(CH_3I)_n^+$ are described in Section 3.2 and Section 3.3. Here, we present a study of $(CH_3I)_n^+$ dissociation that occurs by variable energy electron ionization (EI) ionization. Although this work does not allow filtering of specific cluster sizes before dissociation, it is possible to obtain considerable information regarding size-specific dissociation by scanning the electron energy through dissociative thresholds. There are two other benefits to EI ionization of molecular clusters that we find useful: (i) Unlike MPI, EI ionization is a direct process; therefore, fragment ions that appear in mass spectra can be unambiguously assigned as ionic cluster reactions and not neutral cluster reactions that get subsequently ionized. (ii) EI excitation is tunable over a wide range of energies, thus accessing higher electronic states of the ion. These results greatly assist in the analysis of the resonance photodissociation work that follows.

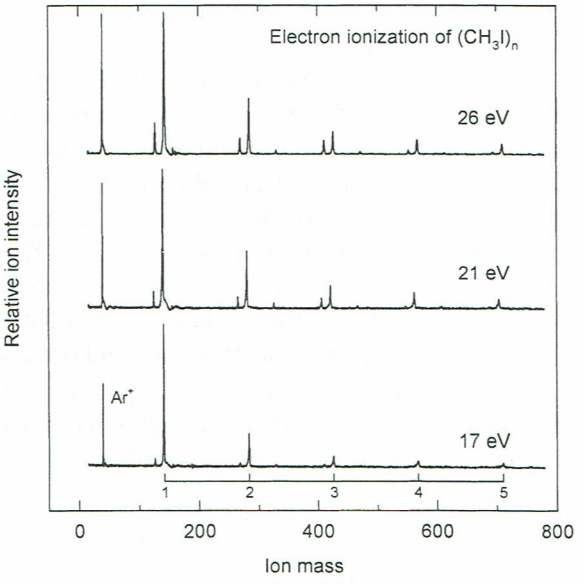

Fig. 3. EI ionization mass spectra of $(CH_3I)_n$ clusters as a function of electron energy. The extent of fragmentation, particularly for CH_3 loss, decreases with electron energy. Interestingly, the relative intensities with n are insensitive to electron energy over this energy range, indicating that they approximate the true cluster size distribution.

The EI/TOFMS of $(CH_3I)_n$ clusters, presented in Fig. 3, reveal some of the prominent $(CH_3I)_n^+$ ion cluster reactions that occur as a function of EI energy. The lack of an active mass filtering technique for EI and dissociation precludes assigning size-specific parentage to reactions that produce ion fragments common to all cluster sizes n, such as I^+ and CH_3^+ in reactions (3) and (5), and, to some extent, fragments from reaction (1). Reactions (2) and (4), on the other hand can be identified with specific values of n with greater confidence. The measure of relative intensities for all observed dissociation channels allows one to sort out multiple routes to the same mass. This turned out to be fairly unambiguous for $(CH_3I)_n$ dissociative ionization, especially since the cluster distribution decreases rapidly with size. In the present case, the ion intensity for successively larger $(CH_3I)_n^+$ clusters decreases by a factor of 3–5. (The deflector plate voltages were adjusted to enhance the signals of larger clusters in Fig. 3). The reaction time was also varied by delaying the ion extraction field with respect to the ionization pulse.

3.1.1. $(CH_3I)_n^+ \rightarrow I(CH_3I)_{n-1}^+ + CH_3$

The demethylation of $(CH_3I)_n^+$ is the most prominent cluster reaction according to Fig. 3. The relative intensities in Fig. 3 attest to the strong dependence on EI energy. These measurements also do not vary with delayed ion extraction, indicating that the reaction is faster than metastable (i.e., $k > 100\ ns^{-1}$) for all cluster sizes and EI energies. Previous studies have indicated that the $CH_3 + I^+$ dissociation correlates with a lower excited electronic state B that is either repulsive or has a shallow minimum (Fig. 4), and that this may be the channel for production of I^+ [9,18]. However, more recent work [14], and the results to follow indicate that the B state undergoes rapid radiationless decay to the A state, which correlates with $CH_3^+ + I$. An interesting feature in the relative reaction cross-section measurements is the enhancement of product observed for dissociative ionization of trimer cation in Fig. 3.

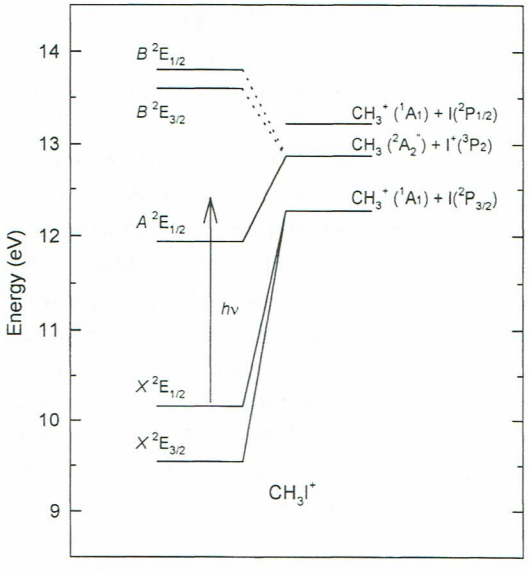

Fig. 4. Energy diagram for CH_3I^+ electronic states and dissociative limits. The dotted lines are previously reported correlations that are unsubstantiated by experiment.

3.1.2. $(CH_3I)_n^+ \rightarrow CH_3(CH_3I)_{n-1}^+ + I$

The monomer (n = 1) dissociation to give $CH_3^+ + I$ has an energy threshold less than that for the reaction yielding $CH_3 + I^+$ (12.24 eV vs. 12.87 eV, respectively, above the neutral ground states) [9,14]. Although the neutral I atom dissociation is extensive for monomer parent ion, the results of Fig. 3 indicate that this reaction becomes insignificant in cluster species. A small yield of $CH_3(CH_3I)_{n-1}^+$ is apparent for n = 2 at high excitation energy, but is essentially non-existent for $n > 2$. It is interesting to speculate whether a cage effect is involved.

3.1.3. $(CH_3I)_n^+ \rightarrow (CH_3I)_{n-1}^+ + CH_3I$

The study of intermolecular dissociation (or evaporation) is not ordinarily reliable without some form of mass selectivity because the parent and fragment cluster ion signals overlap in conventional mass spectra. Nonetheless, the results we present here are informative in so far as the relative ion signal intensities M_{n-1}^+/M_n^+, shown in Fig. 3 are fairly insensitive to EI energy for a wide distribution of cluster sizes n. Intermolecular dissociation is usually recognizable by a distribution that shifts to smaller cluster sizes (i.e., increasing M_{n-1}^+/M_n^+) for increasing EI energy. The extent to which this shift occurs, generally correlates with the cluster ion binding energy.

The production of $I_2^+(CH_3I)_{n-2}$ was observed in lower abundance than that observed by Garvey and coworkers [19]. A likely explanation is that our cluster distributions are weighed toward smaller clusters, and our electron ionization energies are less. We observed proportionately more $I_2^+(CH_3I)_{n-2}$ at higher electron energies. There is also the possibility that some ionization occurs by an intracluster Penning ionization involving Ar [20]. However, this mechanism is expected to be minor, since we observe no $(Ar)_m(CH_3I)_n^+$, and the EI spectra are essentially the same for Ar and He carrier gas. Apparently our expansion conditions are warmer than those obtained in other work [19,20].

3.2. CH_3I^+ and $(CH_3I)_2^+$ photodissociation excitation spectra

The relevant electronic states of CH_3I^+ and of the photofragments for this study are summarized in Fig. 4. EI populates a distribution of the lower electronic states of $(CH_3I)_n^+$. Photodissociation measurements in this work involve the resonant single-photon transition $A\ ^2E_{1/2} \leftarrow X\ ^2E_{1/2}$. The $A\ ^2E_{1/2}$ is predissociative for excitation above the $CH_3^+(^1A_1) + I(^2P_{3/2})$ dissociative limit of the X state. For monomer CH_3I^+ this threshold occurs at about 595 nm, as evidenced in Fig. 5(a). An extensive study of this excitation region has been reported by Walter et al. [14]. The CH_3I^+

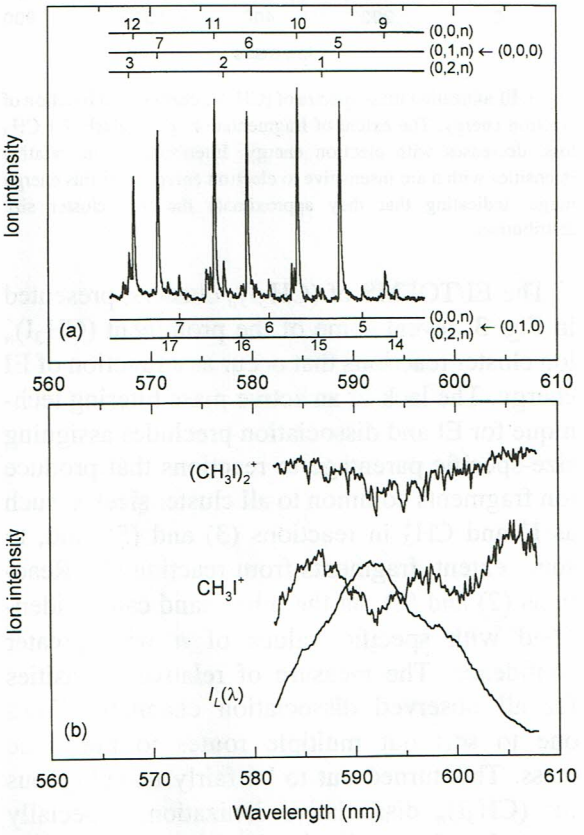

Fig. 5. Resonant ion dissociation spectra of $(CH_3I)_n^+$ for $A\ ^2E_{1/2} \leftarrow X\ ^2E_{1/2}$ excitation. (a) Monomer cation spectrum. CH_3^+ fragment mass detected against a zero background under LMF mode. The vibrations (ν_1, ν_2, ν_3) correspond to symmetric C–H stretch, umbrella, and C–I stretch, respectively. (b) Cluster ion spectrum, dominated by n=2, measured by ion loss of $(CH_3I)_2^+$ and ion formation of $(CH_3I)^+$.

excitation spectrum consists of a series of narrow lines corresponding to excitation of the umbrella (ν_2) and C–I stretch (ν_3) modes.

$A \leftarrow X$ photoexcitation of $(CH_3I)_2^+$ and larger cluster ions resulted primarily in intermolecular dissociation. There was no evidence of C–I bond breaking that is so prominent for CH_3I^+ monomer photodissociation. The photofragment excitation spectrum of $(CH_3I)_2^+$ in Fig. 5(b) was recorded by detecting parent $(CH_3I)_2^+$ (ion dip) and fragment CH_3I^+ (ion formation). The latter spectrum was normalized to the laser intensity $I_L(\lambda)$. The sharp resonant photodissociation features observed for the CH_3I^+ excitation spectrum in Fig. 5(a) are absent for the $(CH_3I)_2^+$ excitation spectrum. A broad, mostly structureless, spectrum is observed that extends well beyond the low energy limit for one-photon dissociation of monomer CH_3I to CH_3 + I. At these longer wavelengths the intermolecular dissociation is the only energetically feasible dissociation. However, at shorter wavelengths, the energetically allowed C–I bond dissociation, which is prominent for the monomer CH_3I (Fig. 6), is essentially quenched in favor of intermolecular bond dissociation. Apparently, the weaker intermolecular bond dissociates preferentially and leaves insufficient internal energy in the monomer fragment ion CH_3I to dissociate the C–I bond. The dimer cation excitation spectrum in Fig. 5(b) exhibits a broad structure (for CH_3I^+ photofragment detection). The spacing is about 275 cm^{-1}, which closely matches the ν_3 C–I stretch frequency in the cation A state [14]. However, this assignment is tentative because the signal-to-noise ratio is low, the laser power wavelength dependence is not smooth, and the structure should be more complicated, in analogy to the monomer spectrum in Fig. 5(a). The apparent sharp structure in the $(CH_3I)_2^+$ ion dip spectrum in Fig. 5(b) could not be reproduced and, therefore, is concluded to be noise.

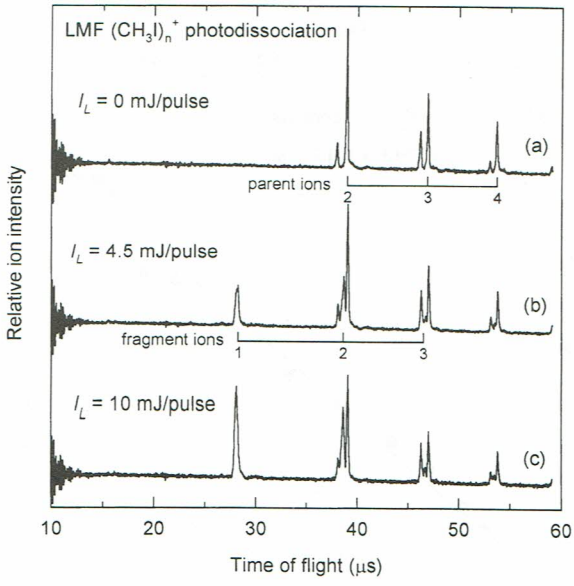

Fig. 6. Photodissociation of $(CH_3I)_n^+$ at 532 nm. The LMF rejects ion masses below the dimer cation, [S(200)]. Fragment spectra are shown for different photolysis pulse energies. Fragment ions of same mass as parent ions may be offset from overlapping by varying the delay between P2 and L (see Fig. 1).

An attempt was made to measure the vibrational distribution in the CH_3I^+ fragment for $(CH_3I)_2^+$ photodissociation by monitoring CH_3^+ fragment by the two step scheme $(CH_3I)_2^+ + h\nu \rightarrow CH_3I^+(v)$ and $CH_3I^+(v) + h\nu \rightarrow CH_3^+$. These single laser pulse experiments, however, failed to reveal any significant appearance of CH_3^+, indicating that the dimer photodissociation lifetime is not less than the laser pulse duration of 5 ns. Interestingly, the measured lifetimes for C–I bond cleavage in CH_3I (about 100 ns) [14] are not significantly longer than the cluster intermolecular bond lifetimes. Hence, one might at first expect to see evidence of C–I bond breaking in the cluster ion photodissociations. The complete absence of this channel is consistent with a cluster ion predissociation mechanism in which the rate limiting step is radiationless decay to vibrationally excited levels of the ground electronic state, followed by a intermolecular dissociation that is considerably faster than C–I bond dissociation. Studies of the A to X radiationless transition would be very helpful toward understanding these dynamics [21,22].

3.3. Size-specific cluster ion photodissociation

In this section, we present results leading to determinations of the cross-sections for $A \leftarrow X$ excitation in the cluster ions and elucidation of a two-photon (or multiphoton) channel that becomes prominent at high laser pulse energy (see Section 4). An instructive way to obtain general information about cluster ion photodissociation is to simply compare cluster ion mass spectra with and without irradiation. Our size-specific results are presented shortly, however, the 532 nm photodissociation results in Fig. 6, in which we filter out ions below mass 200, provide useful guidelines. We have taken the additional step of delaying the photodissociation pulse from the ionizing EI pulse in order to distinguish photofragments from ionization fragments of the same mass (Fig. 6(b)). The spectrum in Fig. 6(c) reveals the increase of photoproduct signal and the corresponding decrease in parent ion signals. By this simple means, a number of interesting observations can be made:

1. The only cluster ion photodissociation that occurs is cleavage of the intermolecular bond

$$(CH_3I)_n^+ \rightarrow (CH_3I)_{n-m}^+ + m(CH_3I)$$

2. The relative cross-section for intermolecular photodissociation, as measured by the M_{n-1}^+/M_n^+, increases with n.
3. The initially formed cluster ion fragments $I(CH_3I)_n^+$ do not absorb or photodissociate in the 580–600 nm region.

The photodissociation mechanism from *specific* parent cluster ions are not easily derivable from spectra such as Fig. 6. The tunable low mass filter (LMF) provides a convenient means of unraveling the chemistry of cluster ions. This method removes successively larger parent cluster ions prior to photodissociation. The difference between successive mass spectra provides the photofragment spectrum for a specific parent cluster ion. In the following we establish the possible values of m for specific values of n as well as identify one- and two-photon dissociation channels.

A means for studying photodissociation from specific cluster ion sizes was illustrated in Fig. 2 for $(CH_3I)_2^+$. Photodissociation by resonant 595 nm pulses gives rise to the intermolecular dissociation $CH_3I^+ + CH_3I$ as seen in Fig. 2(d). Interestingly, as explained above, the prominent monomer cation dissociation $CH_3I^+ \rightarrow CH_3 + I^+$ is not observed in the dimer cation. The LMF of successively larger values of cluster ion sizes n reveals that CH_3I^+ is also produced by one-photon absorption in the dimer and trimer, but only by two-photon absorption in tetramer and pentamer [8]. Photofragment cluster ions are also produced from larger cluster ions. Measurements were made of fragmentation of specific parent cluster ions of size n to cluster ion fragments of size $n-m$. The intensity of the fragment signal was recorded as a function of pulse energy (and converted to photon flux) and the results are presented in Figs. 7–9 for $n = 2$–4, respectively. Generally, a linear dependence on laser power

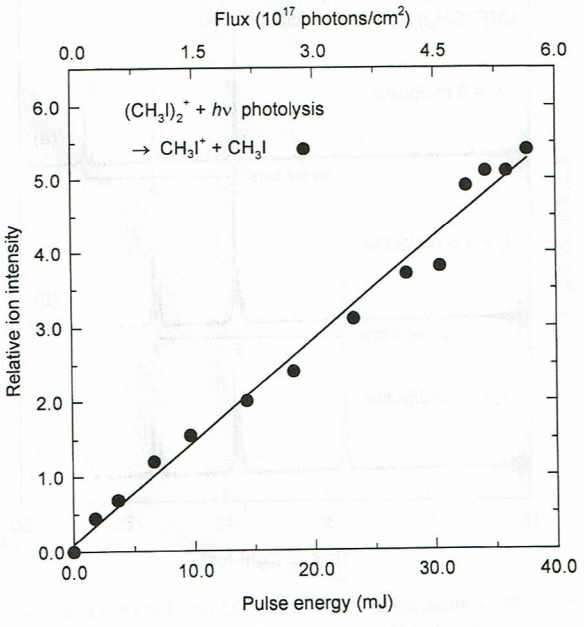

Fig. 7. Mass-resolved photodissociation of $(CH_3I)_2^+$ at 595.2 nm. Dependence of fragment ion signal on laser pulse energy and photon flux.

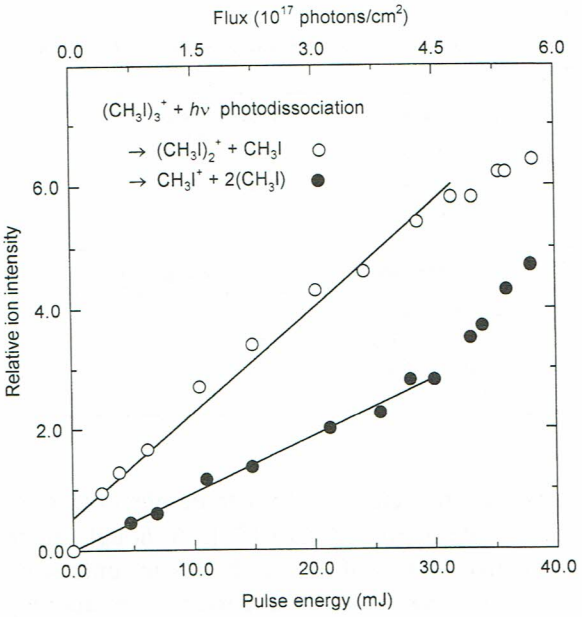

Fig. 8. Mass-resolved photodissociation of $(CH_3I)_3^+$ at 595.2 nm. Dependence of fragment ion signals on laser pulse energy and photon flux. First order equations are fitted to the linear parts of the data.

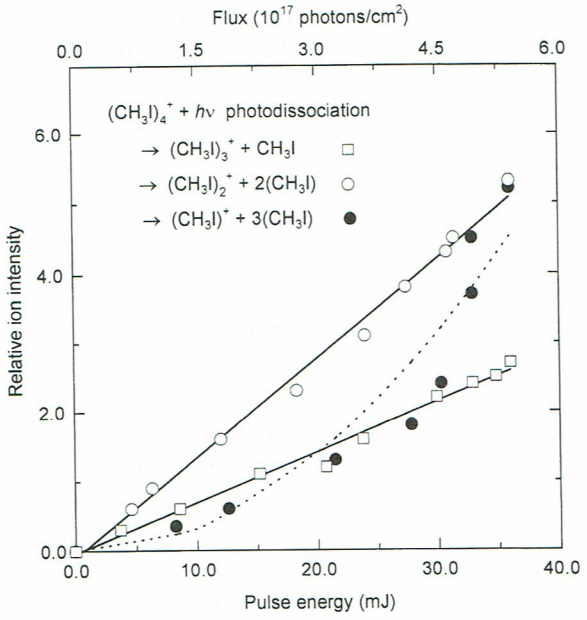

Fig. 9. Mass-resolved photodissociation of $(CH_3I)_4^+$ at 595.2 nm. Dependence of fragment ion signals on laser pulse energy and photon flux. The nonlinear behavior for the CH_3I^+ fragment signal is fitted to a sum of first and second order equations. The curve is for illustrative purposes only.

was observed indicating a one-photon dissociation. However, deviations of this behavior were observed for trimer cations. The cluster ion intermolecular photodissociation pathways are summarized in Table 1.

4. Discussion

4.1. Photodissociation cross-sections

By adjusting the laser beam diameter to exactly overlap the ionization volume for producing parent cluster ions, it is possible to determine the photodissociation cross-sections from ion dip measurements of the parent cluster ion signal. We use the equation

$$\frac{I}{I_0} = \exp(-\sigma F)$$

where I and I_0 are the parent cluster ion signals in the presence and absence of the photodissociation pulse, σ (cm^2) his the photodissociation cross-section and F (photons cm^{-2}) is the photon flux. At the highest photon flux levels (around 5×10^{17} cm^{-2}, see Figs. 7–9), we observed a maximum parent cluster ion depletion of about 25% at 595 nm and 50% at 532 nm. The photodissociation cross-sections measured for $(CH_3I)_2^+$ are $\sigma(595\text{ nm}) = 6 \times 10^{-19}$ cm^2 and $\sigma(532\text{ nm}) = 1.7 \times 10^{-18}$ cm^2. The photodissociation cross-section increases slightly with cluster size. We observed about a 50% greater cross-section at $n = 5$ for 595 and 532 nm excitation. The error limits on the

Table 1
intermolecular photodissociation pathways for $(CH_3I)_n^+ \rightarrow (CH_3I)_{n-m}^+ + (CH_3I)_n$

n	m	
2	1	1-photon
3	1,2	1-photon
4	1	2-photon
	2,3	1-photon
5	1	2-photon
	2,3,4	1-photon

absolute values quoted are estimated to be about a factor of two, mostly due to uncertainty in the overlap of the laser beam with the ionization volume.

4.2. Multiphoton dissociation

Walter et al. achieved efficient 1 + 1 resonant two-photon pumping of the $A \leftarrow X$ and $B \leftarrow A$ transitions in recording photofragment excitation spectra of CH_3I^+ monomer cation [14]. Our cluster ion photodissociation results also show evidence of two or more resonant photon absorption. In the Walter et al experiments, the 1 + 1 two-photon photofragments from the presumed B state were the same as the one-photon photoproducts from the A state, namely $I + CH_3^+$. These investigators reasoned that the B state undergoes rapid radiationless decay to the A state and, therefore, should have the same final chemistry. The two-photon dissociation in the cluster ions leads only to intermolecular dissociation, despite the higher excitation energy relative to the one-photon excitation. So although cluster ions dissociate differently than monomer ions, the chemistry does not change in going from the one-photon to the two-photon level. This is consistent with the previous notion that the B state decays rapidly to the A state.

The one- and two-photon dissociations of $(CH_3I)_n^+$ cluster ions lead to different fragment cluster ions. These are summarized in Table 1. To try to understand the mechanism, we examine the energetics of the dissociations more closely. The C–I bond energy for neutral and ionic methyl iodide are 2.3 eV [23] and 2.73 eV [15]. The intermolecular cluster bond energies are more difficult to estimate. Vaida and coworkers estimate a neutral dimer bond energy of about 0.25 eV [24]. The dimer cluster ion, to our knowledge is not known. However, we estimate it to be about 1 eV for the following reasons: ion–neutral bonds are much stronger than neutral–neutral bonds due to ion-induced dipole interactions. The $(CH_3I)_2^+$ dimer ion core has covalent character due to a three-electron, two-center interaction (3e,2c) [25]. Although, there are many studies of (3e,2c) bonds in ionic solutions, we draw from our experiences in studying the gas-phase $(CH_3SCH_3)_2^+$ dimer cation, which has a (3e,2c) bond strength of about 1 eV [25,26]. Finally, the stepwise binding energies $(CH_3I)_n^+ \rightarrow (CH_3I)_{n-1}^+ + CH_3I$ are not known. These will lie between the ionic and neutral dimer bond energies. For convenience, we estimate that these energies are 0.75 eV for $n = 3$ and 0.50 eV for $n = 4$. From these simple considerations, we obtain the estimates of the energetics for dissociation of $(CH_3I)_n^+$ in Table 2.

Table 2
Rough estimates of the relative energies for cluster ion photodissociation

$(CH_3I)_3^+$ photodissociation	Relative energy (eV)
$(CH_3I)_2^+ + CH_3I$ (6a)	0.75
$CH_3I^+ + (CH_3I)_2$ (6b)	1.50
$CH_3I^+ + 2CH_3I$ (6c)	1.75
$(CH_3I)_4^+$ photodissociation	**Relative energy (eV)**
$(CH_3I)_3^+ + CH_3I$ (7a)	0.50
$(CH_3I)_2^+ + (CH_3I)_2$ (7b)	1.00
$CH_3I^+ + (CH_3I)_3$ (7c)	1.75
$CH_3I^+ + 3CH_3I$ (7d)	2.25

An inspection of Figs. 7–9 reveals that multiphoton effects become evident at about 4.5×10^{17} photons cm^{-2}. This is not evident for $(CH_3I)_2^+$ because there is only one possible dissociation limit. For trimer and tetramer cluster ions, the different possible product channels give added sensitivity to observing multiphoton channels. For trimer cation dissociation, one observes a region of linear increase in the $(CH_3I)_2^+$ and CH_3I^+ signals with photon flux, followed by an apparent two-photon contribution that increases the latter fragment at the expense of the former. At 595 nm, the photon energy available for dissociation is 2.08 eV and 4.16 eV for one- and two-photon excitation. All channels for trimer cation dissociation in Table 2 [reactions (6a)–(6c)] are accessible at the one-photon

level, however, two-photon absorption would change the branching ratio by enhancing the yield of the higher energy dissociation channel, as is observed. For tetramer cation dissociation, the strongest signal is for $(CH_3I)_2^+$ fragment rather than the lower energy $(CH_3I)_3^+$ fragment. This result strongly suggests a single-bond cleavage, rather than an evaporation of two CH_3I molecules. The CH_3I^+ photofragment shows a strong higher-order dependence on photon flux. The dependence of signal on photon flux does not fit well to a binomial equation, suggesting possible multiphoton absorptions or some complicated path, possibly involving some absorption by fragments (see below).

The question whether the second photon is absorbed by the cluster ion before dissociation or fragment cluster ions that further dissociate is answered by our dimer cation results. The $(CH_3I)_2^+$ photodissociation results showed that the CH_3I^+ fragment could not be dissociated, indicating that parent cluster ion dissociation takes place on a timescale that is not less than the 5 ns laser pulse. If this trend holds for larger cluster ions, then the multiphoton absorptions take place in the parent cluster ions.

5. Summary

In this work we have presented a study of the size-specific photodissociation of $(CH_3I)_n^+$ cluster ions. The main conclusions are summarized as follows:

1. For EI/dissociation, reaction (2) is significant for all n studied, reaction (4) is significant only for $n \leq 2$. Reaction (1) occurs for all n, however, the extent of reaction is difficult to measure.
2. For $A \leftarrow X$ photoexcitation of $(CH_3I)_n^+$, reaction (4) dominates for $n = 1$ and is absent for $n > 1$, being replaced exclusively by the intermolecular dissociation reactions (1).
3. The photofragment excitation spectrum is well-resolved for CH_3I^+ but is essentially structureless for $(CH_3I)_2^+$.
4. The photodissociation cross-sections measured for $(CH_3I)_2^+$ are $\sigma(595\ \text{nm}) = 6 \times 10^{-19}\ \text{cm}^2$ and $\sigma(532\ \text{nm}) = 1.7 \times 10^{-18}\ \text{cm}^2$. These values increase moderately with n and are about 50–100% larger at $n = 5$ than at $n = 2$.
5. Efficient resonant multiphoton dissociation occurs for $(CH_3I)_n^+$ photodissociation; however, the higher energy electronic state, presumed to be B, still leads only to intermolecular bond breaking, but shedding additional CH_3I units.

References

[1] J.I. Brauman, Science, 271 (1996) 889, and references cited therein.
[2] J.A. Syage, J. Phys. Chem., 99 (1995) 5772, and references cited therein.
[3] O. Cheshnovsky and S. Leutwyler, J. Chem. Phys., 88, (1988) 4127; O. Cheshnovsky and S. Leutwyler, Chem. Phys. Lett., 121 (1985) 1.
[4] B. Brutschy, C. Janes and J. Eggert, Ber. Bunsenges, Phys. Chem., 92, (1988) 74.
[5] O Echt, P.D. Dao, S. Morgan and A.W. Castleman, Jr., J. Chem. Phys. 82, 4076 (1985); R.G. Kersee and A.W. Castleman, Jr. In: J.P. Maier (ed.), Ion and Cluster Ion Spectroscopy and Structure, Elsevier, New York, 1989.
[6] J.A. Syage and J. Steadman, Rev. Sci. Instrum., 61 (1990) 1204.
[7] J.A. Syage, J.E. Pollard and J. Steadman, Chem. Phys. Lett., 161 (1989) 103.
[8] J.A. Syage, J. Chem. Phys., 92 (1990) 1804.
[9] J.H.D. Eland, R. Frey, A. Kuestler, H. Schulte and B. Brehm, Int. J. Mass Spectrom. Ion Phys., 22 (1976) 155.
[10] D.M. Mintz and T. Baer, J. Chem. Phys., 65 (1976) 2407.
[11] S.P. Goss, D.C. McGilvery, J.D. Morrison and D.L. Smith, J. Chem. Phys., 75 (1981) 1820.
[12] D.M. Szaflarski and M.A. El-Sayed, J. Phys. Chem., 92 (1988) 2234.
[13] M. Kawasaki, H. Sato, T. Kikuchi, S. Kobayashi and T. Arikawa, J. Chem. Phys., 87 (1987) 5739; M. Tadjeddine, G. Bouchoux, L. Malegat, J. Durup, C. Pernot and J. Weiner, Chem. Phys., 69 (1982) 229.
[14] K. Walter, R. Weinkauf, U. Boesl and E.W. Schlag, J. Chem. Phys., 89 (1988) 1914; R. Weinkauf, K. Walter, U. Boesl and E.W. Schlag, Chem. Phys. Lett., 141 (1987) 267.
[15] A.M. Woodward, S.D. Colson, W.A. Chupka and M.G. White, J. Phys. Chem., 90 (1986) 274; W.A. Chupka, S.D. Colson, M.S. Seaver and A.M. Woodward, Chem. Phys. Lett., 95 (1983) 171.
[16] J.A. Syage, J. Chem. Phys., 97 (1992) 6072; J.A. Syage, Phys. Rev. A., 46 (1992) 5666.

[17] W.C. Wiley and I.H. McLaren, Rev. Sci. Instrum., 26 (1955) 1150.
[18] M. Tadjeddine, J.P. Flament and C. Teichteil, Chem. Phys., 124 (1988) 13.
[19] G. Vaidyanathan, M.Y.M. Lyktey, J.J. Stry, R.L. DeLeon and J.F. Garvey, J. Phys. Chem., 98 (1994) 7475.
[20] G. Vaidyanathan, M.T. Coolbaugh and J.F. Garvey, J. Phys. Chem. 96 (1992) 1589.
[21] M.H.M. Janssen, M. Dantus, H. Guo and A.H. Zewail, Chem. Phys. Lett., 214 (1993) 281.
[22] J.A. Syage and J. Steadman, Chem. Phys. Lett., 166 (1990) 159.
[23] R.K. Sparks, K. Shobatake, L.R. Carlson and Y.T. Lee, J. Chem. Phys., 75 (1981) 3838.
[24] D.J. Donaldson, V. Vaida and R. Naaman, J. Chem. Phys., 87 (1987) 2522.
[25] A.J. Illies, P. Livant and M.L. McKee, Mol. Phys., 110 (1988) 7980.
[26] J.A. Syage, J.E. Pollard and R.B. Cohen, J. Phys. Chem., 95 (1991) 8560.